PCCP

RSC Publishing

PAPER

View Article Online
View Journal | View Issue

Cite this: *Phys. Chem. Chem. Phys.*, 2013, **15**, 10904

Hierarchical CuO nanoflowers: water-required synthesis and their application in a nonenzymatic glucose biosensor†

Shaodong Sun, Xiaozhe Zhang, Yuexia Sun, Shengchun Yang, Xiaoping Song and Zhimao Yang*

Received 1st March 2013,
Accepted 23rd April 2013

DOI: 10.1039/c3cp50922b

www.rsc.org/pccp

For the first time, a facile, one-pot water/ethanol solution-phase transformation of $Cu_2(NO_3)(OH)_3$ precursors into bicomponent CuO hierarchical nanoflowers is demonstrated by a sequential *in situ* dissolution–precipitation formation mechanism. The first stage produces a precursory crystal (monoclinic $Cu_2(NO_3)(OH)_3$) that is transformed into monoclinic CuO nanoflowers during the following stage. Water is a required reactant, and the morphology-controlled growth of CuO nanostructures can be readily achieved by adjusting the volume ratio between water and ethanol. Such a bicomponent CuO hierarchical nanoflower serving as a promising electrode material for a nonenzymatic glucose biosensor shows higher sensitivity and excellent selectivity. The findings reveal that the different $Cu_xM_y(OH)_z$ (M = acidic radical) precursors synthesized in a water/ethanol reaction environment can be utilized to obtain new forms of CuO nanomaterials, and this unique water-dependent precursor-transformation method may be used to effectively control the growth of other metal oxide nanostructures.

1. Introduction

Hierarchically nanostructured materials with a large surface area, good conductivity and permeability have become a class of significant functional materials for many emerging research fields, especially environmental remediation, sensor, and energy conversion.[1] The performance of such materials has long been known to be dependent on their size, composition, morphology, structure, crystal phases and crystal facets.[2] To accurately manipulate the above features of the building blocks of hierarchical nanostructures is still necessary because a thorough understanding of the formation mechanism and growth process has important scientific value. Especially, structure- and size-tailoring of the building blocks has been an exciting challenge for bottom-up technology owing to their special structure- and size-dependent effects. Therefore, it is still a challenge to develop new facile synthesis strategies to achieve the controlled synthesis of the building blocks of hierarchical nanostructures.

The synthesis of metal oxide hierarchical nanostructures is of considerable interest because their fundamental properties make them useful in many technological applications.[3] Due to the structural variety and stability of metal oxides, they are currently regarded as the best supports for heterogeneous catalysts.[4] In addition, the multiple oxidation states of metal components provide intriguing catalytic properties to redox reactions. Recently, Lee *et al.* have demonstrated that electrodes made of metal oxides exhibit remarkable electrochemical performances when used in glucose sensors.[5] Cupric oxide (CuO), as a well-known p-type semiconductor material, exhibits great potential for wide applications in photo-electric chemical materials,[6] sensors,[7] anode materials for Li ion batteries,[8–10] supercapacitors,[11] field-emission emitters,[12] CO oxidation,[13] and heterogeneous catalysts for olefin epoxidation,[14] owing to its low band-gap energy (1.2–1.8 eV) and high chemical activity, as well as to its nontoxic nature and low price.[15–17] In the past several years, intensive research has focused on the shape-controlled synthesis of CuO nano- and microstructures, including nanoellipsoids,[18] nanoribbons,[19] nanorods,[20] nanotubes,[21] nanospheres,[22] nanocages,[23] nanoplates,[24] microworms,[25] microflowers,[26] microurchins,[27] and nanowalnuts.[28] However, catalytic, sensing, or photovoltaic activity often depends on the chemical activity, thus hierarchical materials assembled from multicomponent building blocks have been shown to be excellent candidates for these applications.[29,30] In this regard, the further

School of Science, State Key Laboratory for Mechanical Behavior of Materials, MOE Key Laboratory for Non-Equilibrium Synthesis and Modulation of Condensed Matter, Xi'an Jiaotong University, Xi'an 710049, ShaanXi, People's Republic of China. E-mail: zmyang@mail.xjtu.edu.cn

† Electronic supplementary information (ESI) available: Additional FTIR spectra, XRD patterns, TEM images, BET data and Table S1. See DOI: 10.1039/c3cp50922b

assembly of different nanosubunits into CuO hierarchical structures has also been reported recently.[31–33] For example, a three-dimensional (3D) hierarchical CuO dandelions assembly of rhombic nanoribbons was prepared by a solvent hydrothermal route in the presence of ethanol.[31] 3D CuO ellipsoids composed of a hundred one-dimensional (1D) nanoparticles were synthesized by a facile solution oxidative route under the assistance of formamide.[32] Two-dimensional (2D) CuO mesoplates have been synthesized using a mild solution in the presence of tetrabutylammonium hydroxide.[33] However, these hierarchical structures always possess onefold building blocks, namely, the building block was usually a single crystalline feature. In an attempt to further improve the surface area, a new category of hierarchical CuO nanocrystals with multicomponent (polycrystalline or mesocrystalline) building blocks was developed. To date, the relevant experimental investigation is still unavailable. Hence, there is still much room for progress with regard to the development of novel CuO hierarchical nanostructures, particularly in terms of large-scale green synthesis and multicomponent nanosubunits.

A recently demonstrated top-down precursor-transformation approach by Liu has proven to be a typically successful means to effectively achieve the synthesis of bicomponent CuO hierarchical nanocrystals by annealing of copper hydroxide nitrate ($Cu_2(OH)_3NO_3$) precursors,[34] because $Cu_2(OH)_3NO_3$ is considered to be a good precursor for the *in situ* synthesis of hierarchical CuO structures.[28,34,35] Over the past decades, many solution synthesis routes have been employed to synthesize $Cu_2(OH)_3NO_3$ crystals. For instance, Peng and coworkers have synthesized $Cu_2(OH)_3NO_3$ nanoribbons by aging a mixed solution of $Cu(NO_{3)2}$ and aminoethanol.[28] Liu has fabricated $Cu_2(OH)_3NO_3$ urchins composed of 1D nanorods and nanobelts by aging a mixed solution of $Cu(NO_3)_2$ and 2-propanol.[34] Matijević and coworkers have prepared $Cu_2(OH)_3NO_3$ hexagonal platelets by aging a mixed solution of $Cu(NO_3)_2$ and NaOH.[35] Based on these $Cu_2(OH)_3NO_3$ precursors, elaborate tailoring of experimental parameters such as reactant concentrations, reaction temperature, reaction time, reaction environment and subsequent annealing temperature can be achieved for the controlled transformation from $Cu_2(OH)_3NO_3$ to CuO crystals.[28,34,35] Although the aforementioned methods are successful in preparing CuO crystals by the *in situ* precursor-transformation approach at a higher annealing temperature, the sizes of these hierarchical CuO structures are limited to the micrometer or sub-micrometer scale and the building blocks are usually single crystalline, and therefore could not offer larger interfacial areas for catalyst, sensor and energy conversion. To the best of my knowledge, no method has been reported to date for the one-pot solution-phase transformation of $Cu_2(NO_3)(OH)_3$ precursors into hierarchical CuO nanostructures without a trace of the subsequent annealing treatment in air.

Herein, we report, for the first time, a facile, one-pot solution-phase transformation of $Cu_2(NO_3)(OH)_3$ precursors to directly synthesize well-defined 3D nanoparticle-aggregated bicomponent CuO hierarchical nanoflowers without annealing treatment in air. A systematic investigation was carried out to confirm the water-dependent formation mechanism of the bicomponent CuO hierarchical nanoflowers by *in situ* transformation of the $Cu_2(NO_3)(OH)_3$ crystals. The study is of great significance in one-pot synthesis of highly active nanostructures, and provides a good opportunity to understand the fundamental importance of the investigation of the formation mechanism and growth process of hierarchical CuO nanostructures with controllable aggregation-based behaviours. In addition, we further demonstrated that such a hierarchical CuO nanoflower could serve as a promising probe material for enhancing non-enzymatic glucose sensing.

2. Experimental section

2.1 Chemicals

$Cu(NO_3)_2$ and NaOH were obtained from Aladdin reagent. All chemicals used in our experiment were of analytical grade and used without further purification. Deionized water (18.2 MΩ cm) from a Milli-Q Academic water purification system (Millipore Corp.) was used in all preparations.

2.2 Synthesis of bicomponent CuO hierarchical nanoflowers

In a typical procedure, $Cu(NO_3)_2$ (0.12 mmol) was dissolved in ultrapure water (2 mL) in a beaker under constant stirring for 5 min at room temperature. And then ethanol (30 mL) was added to the copper salt solution. Afterwards, the above solution was stirred at 75 °C for 2 min. A precipitate was produced when a NaOH ethanol solution (0.02 M) was added dropwise to the above solution. After being stirred for 15 min, the precipitates were allowed to cool to room temperature naturally. Afterwards, the obtained products were centrifuged at 10 000 rpm for 2 min (XIANYI TG16-WS centrifuge). The precipitates were centrifuged twice more in anhydrous ethanol and ultrapure water, respectively.

2.3 Characterization

Powder X-ray diffraction (XRD) patterns were recorded on a Bruker-AXS D8 ADVANCE diffractometer operated at 40 kV voltage and 40 mA current using Cu Kα radiation (λ = 1.5406 Å) in the range (20–80°). The chemical composition and purity of the products were examined by electron energy dispersive X-ray (EDX) analysis. Surface analysis for the as-prepared products was performed by X-ray photoelectron spectroscopy (XPS) using an Al mono Kα X-ray source operated at 90 W (England, Kratos Axis Ultra DLD). The vibration property was characterized by a Lab-RAM HR800 Raman spectroscopy instrument. The morphology of the powders was investigated by field-emission scanning electron microscopy (FESEM) using a JEOL (JSM-7000F) instrument at an accelerating voltage of 20 kV. The transmission electron microscopy (TEM) and high resolution transmission electron microscopy (HRTEM) analysis as well as selected-area electron diffraction (SAED) analysis were performed on a JEOL JEM-2100 transmission electron microscope operating at an accelerating voltage of 200 kV. The sample for the TEM analysis was prepared by ultrasonic dispersion for 60 s with ethanol (2 mL) in a 3 mL centrifuge tube. Then, the products were dropped onto a carbon-coated copper grid and dried in air before TEM analysis. Fourier transform infrared spectroscopy (FTIR, AVATER-360B) was carried

out using a potassium bromide (KBr) pellet technique. In making the KBr pellets, around 1 mg of the as-prepared sample was mixed with 100 mg of KBr.

2.4 Preparation of CuO/Nafion/glassy carbon modified electrode and electrochemical measurements

An enzyme-free amperometric electrochemical sensor was prepared by casting Nafion impregnated CuO powders onto a glassy carbon electrode at room temperature. The modified electrode was prepared as follows: 2 mg of the final CuO powders was dispersed in 2 mL Nafion solution (0.05%, Sigma-Aldrich). 20 μL of the suspension with dispersed CuO was dropped on the pre-treated glassy carbon electrode (denoted as CuO/Nafion/GCE), and dried at room temperature. Before modification, the bare GCE of 5.0 mm in diameter was polished to a mirror-like surface with 0.5 μm, 0.05 μm and 50 nm alumina slurry, and then washed ultrasonically in deionized water, 50% (v/v) nitric acid solution, ethanol, and deionized water for a few minutes, respectively. Electrochemical measurements were carried out on an Ametek VMC-4 electrochemical analyzer with a conventional three-electrode system in 0.1 M KOH aqueous solution. The as-prepared CuO/Nafion/GCE was used as the working electrode with a platinum foil as the counter electrode and an Ag/AgCl as the reference electrode.

3. Results and discussion

3.1 Nanoflowers growth

Structural analysis of the as-prepared CuO crystals was investigated by XRD, and the result is shown in Fig. 1a. All the diffraction peaks are indexed according to the standard monoclinic structure of CuO crystal (JCPDS file No. 48-1548). No peaks of impurities such as copper hydroxide nitrate, copper hydroxide, or cuprous oxides were found, suggesting the high purity of the as-obtained product. EDX analysis was also used to characterize the chemical composition, and only copper and oxygen (no nitrogen element) were detected (see Fig. 1b). Further evidence for the composition and purity of these products was obtained by XPS, and the core-level Cu 2p high-resolution photoemission spectrum of the as-prepared nanoflowers is shown in Fig. 1c. According to the previous report,[20] the peaks correspond to the core-level $Cu_{2p1/2}$ and $Cu_{2p3/2}$ transitions of copper at 954.1 and 934.1 eV for the Cu 2p spectrum, respectively. Moreover, the presence of satellites (asterisks) on the higher binding energy sides, which are comparable to the values reported for Cu 2p levels in CuO, further demonstrate that the as-prepared products are pure CuO crystals.[26] Additional structural information was obtained by Raman spectroscopy in the range of 200–700 cm^{-1} measured at room temperature. Fig. 1d displays the corresponding Raman scattering spectrum. Previous reports have demonstrated that the zone center Raman active normal modes of CuO crystals can be described as $\Gamma_{RA} = 4A_u + 5B_u + A_g + 2B_g$. There are three acoustic modes ($A_u + 2B_u$), six infrared active modes ($3A_u + 3B_g$), and three Raman active modes ($Ag + 2B_g$).[36] Generally, the modes at 283, 324, and 613 cm^{-1} for all of the samples can be assigned to the A_g, B_g^1, and B_g^2 modes, respectively, which is consistent with the previous report on CuO crystals.[37] So the aforementioned Raman spectrum indicates that the as-prepared hierarchical CuO nanoflower possesses a single monoclinic phase and is well crystalline.[37]

The morphology and structure characterization of the as-prepared hierarchical CuO nanoflower were further performed by FESEM, TEM and HRTEM as well as SAED investigation, respectively. A low-magnification FESEM image of the as-prepared products is shown in Fig. 2a, it can be seen that the products are flower-like nanostructures and composed of many nanosheet building blocks. Fig. 2b is a typical high-magnification FESEM image, which indicates that the nanoflowers have rough surfaces, and that these sheets exhibit nanometer-sized thickness and nanometer-sized width and length. A statistical analysis of FESEM data reveals that the nanometer-sized dimensions of these nanosheets are relatively uniform, with a size range of 100–300 nm. A typical low-magnification TEM image of the as-prepared hierarchical CuO nanoflowers is shown in Fig. 3a. We can see that the nanoflowers are composed of nanosheet building blocks, and some of these nanosheets have joined together and are disorderly attached to form hierarchical features, in particular there is an extremely strong contrasting between their side-views (dark) and front-views (bright). Fig. 3b is a typical high-magnification TEM image of an individual as-made CuO nanoflower, and it is

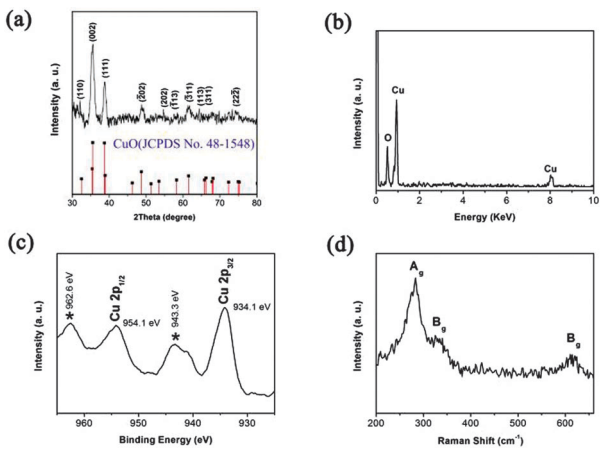

Fig. 1 XRD pattern (a), EDX spectrum (b), Cu 2p core-level XPS spectrum (c), and Raman spectrum (d) of the as-prepared CuO nanoflowers.

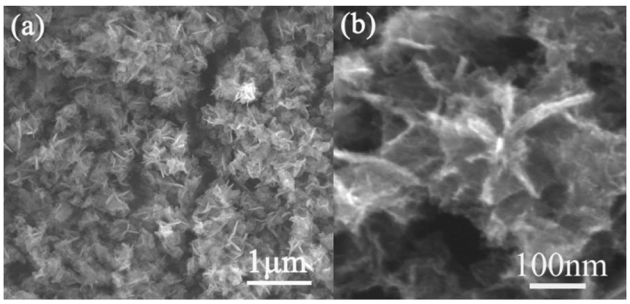

Fig. 2 (a) Low-magnification FESEM image of the as-prepared CuO nanoflowers; (b) high-magnification FESEM image of an individual CuO nanoflower.

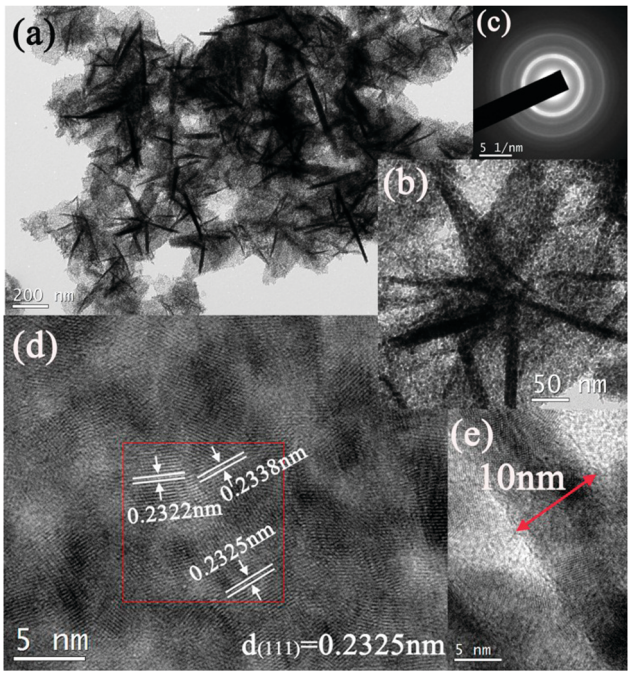

Fig. 3 (a) Low-magnification TEM image of the as-prepared CuO nanoflowers; (b) an individual CuO nanoflower; (c) the corresponding SAED pattern (d) HRTEM image of a nanosheet building blocks; (e) TEM image of a side view of a nanosheet building block.

interestinging to see that the nanosheet building blocks are obviously rough and are made up of an assembly of a large number of nanoparticles and voids, leading to the formation of bicomponent hierarchical nanostructures. Namely, the nanoflower is composed of abundant nanosheet building blocks, and these nanosheet building blocks are an assembly of a large number of nanoparticle subunits, which can be termed as bicomponents of CuO hierarchical nanoflowers. The corresponding SAED pattern of an individual particle is displayed in Fig. 3c, suggesting that the as-prepared bicomponent CuO hierarchical nanoflower possesses a polycrystalline nature. The detailed microstructure of a nanosheet building block was further investigated by HRTEM, as shown in Fig. 3d and e, and the lattice fringes are marked by white lines and arrows. The corresponding lattice spacing of three nanoparticles are 0.2322 nm, 0.2325 nm and 0.2338 nm, respectively, which are in good agreement with the *d* value of the (111) facets of CuO crystal (0.2325 nm). From the HRTEM image (Fig. 3d), it can also be clearly found that the growth directions of these (111) facets are not homogeneous, and the lattice fringes of these nanoparticles are attached (marked with the red square). A side-view TEM image exhibits a nanosheet thickness of about 10.0 nm (Fig. 3e). Based on the above results, the formation of bicomponent CuO hierarchical nanoflowers exposed with many (111) facets was successfully achieved.

3.2 Formation process

TEM and XRD analyses of the as-synthesized products obtained at different reaction stages were performed to investigate the formation process of the bicomponent CuO hierarchical nanoflowers (Fig. 4). Flower-like nanostructures with nanosheet building blocks having size between 100–300 nm were formed with a volume of NaOH of 5 mL (Fig. 4a). This ultrathin individual nanosheet (5–20 nm) was almost transparent under the electron-beam illumination. These well-defined nanosheets were identified to be a new form of precursory crystal (later identified as $Cu_2(NO_3)(OH)_3$). An increased population of the hierarchical nanosheets was observed along with the increase of NaOH, with the disappearance of the smooth $Cu_2(NO_3)(OH)_3$ crystals. The clearly visible spinous nanostructures started to form on the surface of the sheet-shaped $Cu_2(NO_3)(OH)_3$ crystals when the volume of NaOH was increased to 15 mL (Fig. 4b). The observed small-sized irregularly-shaped particles are likely to be the remains of the sheet-shaped $Cu_2(NO_3)(OH)_3$ crystals, suggesting that transformation of the $Cu_2(NO_3)(OH)_3$ crystals had occurred. This could also indicate that the $Cu_2(NO_3)(OH)_3$ crystals served as a type of precursors and their transformation products were the building materials for the formation of the hierarchical nanosheets. The smooth surfaces of these nanosheets further evolved into wholly rough ones after addition of 30 mL NaOH solution (Fig. 4c). When the reaction time was increased to 2 min after full addition of the NaOH solution, the spinous nanostructures gradually evolved into nanoparticle-aggregations (Fig. 4d). This was further supported by the TEM image obtained from the as-prepared bicomponent CuO hierarchical nanoflowers subjected to 15 min of heat preservation at 75 °C, in which the entire nanosheet was covered by densely

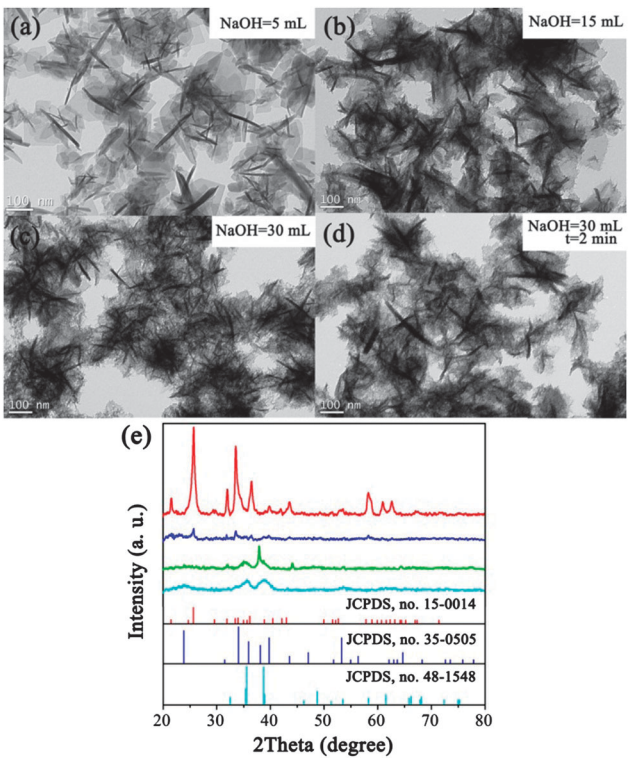

Fig. 4 TEM images of the as-synthesized products obtained at different stages: (a) NaOH = 5 mL; (b) NaOH = 15 mL; (c) NaOH = 30 mL; (d) NaOH = 30 mL and reaction time = 2 min; (e) the corresponding XRD patterns.

populated nanoparticles (Fig. 3). Note that there was almost no change in the sizes and shapes of these new hierarchical crystals compared to the previous $Cu_2(NO_3)(OH)_3$ crystals (Fig. 4a → Fig. 4b → Fig. 4c → Fig. 4d → Fig. 3), suggesting the achievement of one-pot solution-phase *in situ* transformation of $Cu_2(NO_3)(OH)_3$ precursors into bicomponent CuO hierarchical nanoflowers without a trace of the subsequent annealing treatment in air.

Fig. 4e shows the XRD data of the above as-synthesized products at different reaction stages. The XRD pattern (red curve) obtained from the sample after addition of a small amount of NaOH (5 mL) solution was dominated by the $Cu_2(NO_3)(OH)_3$ diffraction peaks (JCPDS file no. 15-0014). No other diffractions due to crystallographic impurities such as CuO, $Cu(OH)_2$ or $Cu(NO_3)_2$ were found. The XRD pattern (blue curve) obtained from the sample containing nanosheets and small numbers of spinous particles (after addition of NaOH = 15 mL) exhibits an obviously weak group of diffraction peaks that suggests the transformation of $Cu_2(OH)_3NO_3$ into intermediate products. The XRD pattern (green curve) obtained from the spinous sheet-shaped crystals (after addition of NaOH = 30 mL) was dominated by the diffraction peaks of orthorhombic $Cu(OH)_2$ (JCPDS file no. 35-0505), while the diffraction peaks belonging to the $Cu_2(OH)_3NO_3$ crystals were further weakened. The XRD pattern (gyan curve) obtained from the sample assembled by small nanoparticles (after addition of NaOH = 30 mL and with a reaction time of 2 min) displays obvious diffraction peaks of monoclinic CuO crystals (JCPDS file no. 48-1548), while the diffraction peaks belonging to the $Cu(OH)_2$ crystals were significantly weakened. The XRD pattern obtained from the sample as shown in Fig. 1a (with 15 min heat preservation) can be indexed to pure monoclinic CuO crystals. These XRD data correspond perfectly to the structural changes observed in the TEM images, thus suggesting a three-stage formation process. The first-stage structural formation process (after addition of NaOH = 5 mL) involves the reaction between $Cu(NO_3)_2$ and NaOH to form the sheet-shaped $Cu_2(OH)_3NO_3$ precursory crystals. The second-stage structural formation process (after addition of NaOH = 15 mL) starts after the $Cu_2(OH)_3NO_3$ precursory crystals reach their maturity. This process involves the rapid dissolution of $Cu_2(OH)_3NO_3$ precursory crystals that is accompanied by a speedy intermediate $Cu(OH)_2$ spinous nanosheets growth process. The third-stage structural formation process (after addition of NaOH = 30 mL and an increase of reaction time) involves the gradual transformation of the $Cu(OH)_2$ intermediate crystals *in situ* into bicomponent CuO hierarchical nanoflowers. A detailed growth process is given in the following discussion.

FTIR spectra, as shown in Fig. S1 (see ESI†), further confirmed that the $Cu_2(OH)_3NO_3$ nanoflowers were completely converted to CuO nanoflowers. Fig. S1a (ESI†) shows the FTIR spectrum of the $Cu_2(OH)_3NO_3$ nanoflowers. The strong peaks at 3546 cm^{-1} and 3422 cm^{-1} correspond to the stretching vibration of the O–H group of molecular water and of hydrogen-bound O–H groups, respectively.[29] The bending vibration of water and adsorbed OH groups leads to the peak at 1626 cm^{-1}.[27] The peaks observed at 679 cm^{-1}, 782 cm^{-1}, 1046 cm^{-1}, 1356 cm^{-1} and 1423 cm^{-1} can be assigned to the vibrational modes of nitrate (NO_3^-) ions.[28–30,34] The bands in the infrared spectrum at below 600 cm^{-1} are due to Cu–O vibrations.[28] However, after heat preservation (15 min), a typical FTIR spectrum of the as-prepared bicomponent CuO hierarchical nanoflowers was obtained as shown in Fig. S1b (ESI†). The peak at 1423 cm^{-1} due to NO_3^- groups decreased significantly. This indicated that NO_3^- groups were removed after the heat treatment of the $Cu_2(OH)_3NO_3$ nanoflowers in solution at 75 °C.

3.3 Growth mechanism

$$2Cu^{2+} + 3OH^- + NO_3^- \rightarrow Cu_2(OH)_3NO_3 \quad (1)$$

$$Cu_2(OH)_3NO_3 + H_2O \rightarrow 2Cu(OH)_2 + HNO_3 \quad (2)$$

$$Cu(OH)_2 + 2OH^- \rightarrow [Cu(OH)_4]^{2-} \quad (3)$$

$$[Cu(OH)_4]^{2-} \rightarrow CuO + 2OH^- + H_2O \quad (4)$$

Based on the above experimental results, the detailed chemical reactions that are involved in the solution-phase growth of bicomponent CuO hierarchical nanoflowers are suggested as follows: initially, by the addition of a small amount of OH^- into $Cu(NO_3)_2$ solution (under weakly acidic conditions), $Cu_2(OH)_3NO_3$ (light blue precipitate) can be formed in the present of NO_3^- (reaction (1)). The formation of the sheet-like structures is due to the nature of the layered crystal structure of $Cu_2(OH)_3NO_3$ as shown in Fig. 5a. The structure can be viewed as layers of octahedral copper stacked on top of each other. The octahedral copper forms layers of stoichiometry $[Cu_2(OH)_3]^+$, and NO_3^- ions are situated between the positive layers for charge balance, these are linked by hydrogen bonding to the hydroxyl groups belonging to the octahedral copper layers. However, these $Cu_2(OH)_3NO_3$ sheets would be slowly converted into divalent $Cu(OH)_2$ in water under an alkaline environment (reaction (2)), because NO_3^- are substituted by a quarter of the OH^- groups along with the increase of NaOH solution. The crystal structure of $Cu(OH)_2$ is shown in Fig. 5b. The Cu–O bonds are established due to the oxolation in the *a–b* plane of $Cu(OH)_2$. Subsequently, the tetrahydroxocuprate(II) anion ($[Cu(OH)_4]^{2-}$) is likely to be formed from the $Cu(OH)_2$ under a strong basic environment (reaction (3)), because of the Jahn–Teller stabilization in square-planar copper(II) complexes.[38] However, $Cu(OH)_2$ is a metastable phase which is easily transformed to the more stable CuO by thermal dehydration in aqueous media,[39] because the solubility of $Cu(OH)_2$ is 1.3×10^{-5} mol L^{-1} which is higher than that of CuO (2×10^{-7} mol L^{-1}).[40] So the loss of water of $Cu(OH)_2$ would be generated by an oxolation process at a relatively higher temperature, the hydrogen bonds which interconnect the $Cu(OH)_2$ precursors are easily destroyed, by a dehydration process and the formation of O–Cu–O bridges. Finally, thermodynamically stable monoclinic CuO crystal crossing bonds of CuO_4 (Fig. 5c) is prepared and precipitated to yield solid particles by the decomposition of $[Cu(OH)_4]^{2-}$ species (reaction (4)).[41] Moreover, it has been reported that a higher pH value can

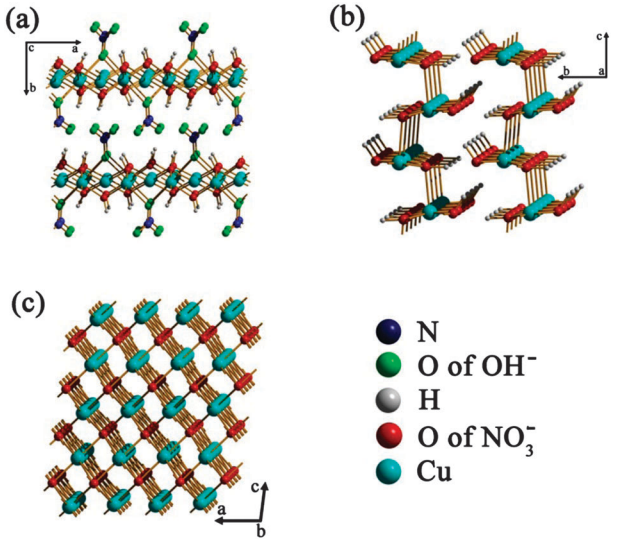

Fig. 5 Crystal structures of $Cu_2(OH)_3NO_3$ (a), $Cu(OH)_2$ (b) and CuO (c).

accelerate the transformation process.[39] In the present work, $Cu_2(OH)_3NO_3$ was formed in a solution of pH value below 6 and transformed to $Cu(OH)_2$ and CuO in a solution of pH value beyond 12. In order to further demonstrate the role of OH^- ions in the formation of CuO crystals, a control experiment was carried out under the same conditions but changing the molar ratio between OH^- and Cu^{2+} ions. The TEM images and XRD patterns of the corresponding products are shown in Fig. S2 and S3 (see ESI†), respectively. From them, we can find that the $Cu_2(OH)_3NO_3$ flower-like nanostructures were formed in a lower basic environment, while CuO nanoflowers can be synthesized in a higher concentration of NaOH. In addition, a relatively higher reaction temperature also played an important role in the *in situ* transformation of $Cu_2(OH)_3NO_3$ precursors into bicomponent CuO hierarchical nanostructures (Fig. S4, see ESI†). The growth of the as-prepared bicomponent CuO hierarchical nanoflowers from $Cu_2(OH)_3NO_3$ precursors could be proposed as follows: CuO seeds or clusters were generated *in situ* from dissolution of the $Cu_2(OH)_3NO_3$ nanoflowers at the initial dehydration stage; in order to minimize the overall energy of the reaction system, primary nanoparticles tended to aggregate rapidly maintaining the *status quo* in the water/ethanol environment; as time progressed, CuO nanoparticles were fused together to finally form the monoclinic CuO nanoflowers (Fig. 3 and 4).

3.4 Control growth

According to the above chemical reactions, the as-prepared bicomponent CuO hierarchical nanoflowers reported here are essentially determined by the characteristics of the $Cu_2(OH)_3NO_3$ precursors. Herein, the formation of $Cu_2(OH)_3NO_3$ species not only depended on the precursor formation temperature and the molar ratio between sodium hydroxide and copper salt but also the volume ratio between water and ethanol. The $Cu_2(OH)_3NO_3$ precursors synthesized in different volume ratios of water and ethanol can modify the reaction process (reactions (2–4)), which might affect the competition between thermodynamics and kinetics during the transformation of precursors, nucleation and growth of CuO crystals.

In the present experiment, the *in situ* transformation from $Cu_2(OH)_3NO_3$ precursors to CuO nanostructures can be affected by the feature of the ethanol capping agent, since the polarity of ethanol is less than that of water, which suggests that the electrical force between any two charges in the ethanol system is much larger, thus the charge-transmission is relatively difficult. The very highly positively charged surface of the $Cu_2(OH)_3NO_3$ suppressed the transformation process.[34] Preferential adsorption easily occurred between the hydroxyl groups of ethanol molecules and the surfaces of $Cu_2(OH)_3NO_3$,[28] resulting in the *in situ* transformation of $Cu_2(OH)_3NO_3$ precursors into CuO crystals by the induction of a small amount of water (reaction (2)). Furthermore, the {111} facets of CuO crystals are formed by both Cu and O atoms, and surface Cu atoms with dangling bonds on the {111} facets can make them positively charged,[42] so the {111} facet can also be strongly protected in an environment containing a high amount of hydroxyl groups,[28] which corresponds perfectly to the structural feature observed in the HRTEM image of the as-prepared bicomponent CuO hierarchical nanoflowers (Fig. 3d). Thus, it is possible that the strain energy is stored in the CuO interfaces during the mass exchange process during the formation of O–Cu–O bridges. Finally, reduction of the surface free energy by fusing and eliminating the high-activity interfaces can drive the spontaneous ordering assembly to form the hierarchical nanosheets from the $Cu_2(OH)_3NO_3$ precursors in the presence of ethanol capping solvent. However, the {111} facet of CuO crystal would be weakly protected by ethanol agent as the amount of water further increased, so the nanoparticle building blocks of nanosheets might grow up to form new stable morphologies. Therefore, we proposed that water was a required reactant for controlling the water/ethanol solution-phase transformation of $Cu_2(OH)_3NO_3$ precursors into CuO nanostructures.

The above mechanistic studies have confirmed the decisive role of water and ethanol molecules for the shape-controlled synthesis of CuO nanostructures in a solution-phase environment. Here, we have successfully converted $Cu_2(OH)_3NO_3$ nanoflowers to different CuO nanostructures by adjusting the volume ratio between water and ethanol, and more dramatic effects were observed with an increase in the amount of water ($V_{ethanol}$ = 30 mL). Irregular net-like structures composed of many nanowires (Fig. 6a) were formed in the absence of water. The corresponding XRD pattern is shown in Fig. 6g (black curve), and the diffraction peaks belonging to the $Cu_2(OH)_3NO_3$ crystals (JCPDS file no. 15-0014) were very weakened. As a small amount of water (1 mL) was added to the ethanol solvent, flower-like CuO hierarchical nanostructures (Fig. 6b) were obviously synthesized (Fig. 6g, purple curve, JCPDS file no. 48-1548). A further increase in the amount of water to 1.5 mL, resulted in the formation of bicomponent CuO hierarchical nanoflowers (Fig. 6c), and the diffraction peaks of CuO crystals increased (Fig. 6g, yellow curve). However, the well-defined flower-like CuO morphology started to change as the amount

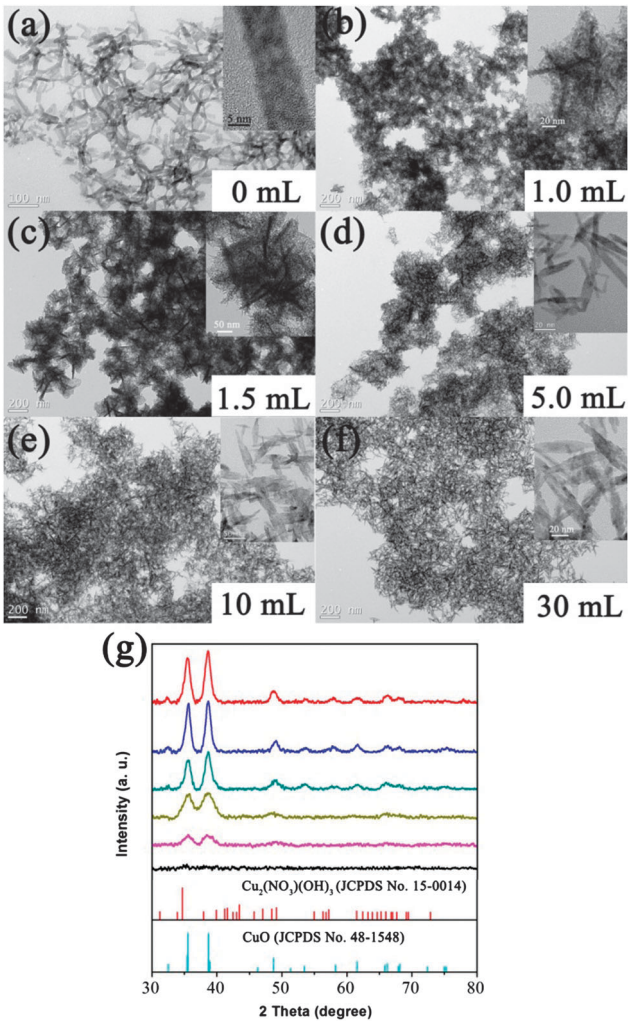

Fig. 6 Different CuO nanostructures obtained in different amounts of water under otherwise the same conditions: (a) in the absence of water; (b) V_{water} = 1 mL; (c) V_{water} = 1.5 mL; (d) V_{water} = 5.0 mL; (e) V_{water} = 10 mL; (f) V_{water} = 30 mL; (g) the corresponding XRD patterns.

of water was enhanced to 5 mL, and a sample assembled from leaf-like structures was formed (Fig. 6d). Similarly, uniform nanoleaves were subsequently obtained by the increase of water (Fig. 6e and f), and the diffraction peaks belonging to the CuO crystals were significantly enhanced (blue curve and red curve, Fig. 6g). A high amount of water in the reaction mixture leads to the fast dissolution and precipitation of $Cu_2(OH)_3NO_3$ as in reaction (2), and the hydroxide-ion concentration also increases the reaction rates, through reactions (3) and (4). But square planar $[Cu(OH)_4]^{2-}$ ions are highly stable inhigh amounts of water, by reducing the growth rate of CuO through the reverse process of reaction (4). The slow CuO growth rate results in the largest single-crystalline-like domains in the leaf-like particles, and a typical HRTEM image (Fig. S5, see ESI†) of the sample as shown in Fig. 6f can support this viewpoint. This process is similar to that described ref. 2. On the contrary, the fast precipitation of CuO in a low amount of water maintains the original flower-like assembly of many nanoparticles with tiny single-crystals (as shown in Fig. 3).

3.5 Glucose sensor

The as-prepared bicomponent CuO hierarchical nanoflowers were employed as glucose sensing anode materials. We have investigated a nonenzymatic glucose sensor by deposition of the aqueous dispersion of CuO powders on a GCE surface. For the investigation of an amperometric biosensor for glucose, the CuO sample was solubilized in Nafion, a perfluorosulfonated polymer, to facilitate the modification of the GCE surface (denoted as CuO/Nafion/GCE).[43] Linear sweep voltammograms (LSV) were measured to examine the catalytic activity of the modified CuO/Nafion/GCE towards glucose oxidation in a 0.1 M KOH solution in the presence of different concentrations of glucose at a scan rate of 0.02 V s^{-1} (Fig. 7a). We have performed a control experiment by investigating the CV behavior of CuO/Nafion/GCE in the absence of glucose. As expected, it was found that the current signal of CuO/Nafion/GCE towards the oxidation of glucose was weak (see black curve). In contrast, the amperometric response will increase with the enhancement of glucose concentration at all applied potentials. The as-prepared bicomponent CuO hierarchical nanoflowers can exhibit a remarkable catalytic current peak about 108.4 μA in an intensity of +0.50 V (see purple curve).

Fig. 7b shows the typical current-time response plot of the as-prepared CuO/Nafion/GCE in 0.1 M KOH solution with successive stepwise change of the glucose concentrations. The solution was vigorously stirred to guarantee good mixing of glucose with the electrolyte and to obtain an homogeneous glucose concentration instantly. When an aliquot of glucose solution was added to the KOH solution with stirring, the as-prepared CuO/Nafion/GCE responded instantly to the substrate and the current increased steeply to reach a stable value. The amperometric response displays a step-like enhancement in accordance with a stepwise addition of glucose. The signal noise increases with the enhancement of glucose concentration which is because of the accumulation of absorbed intermediate species on the electrode surfaces.[44]

Fig. 7c shows the corresponding calibration curve of the CuO glucose sensor based on the amperometric results. It shows a linear region in a range of concentrations between 10 μM and 5 mM. The fitting equation is I (μA) = 4.089 + 0.5214 C (μM) with a correlation coefficient of 0.9991. The sensitivity of the present non-enzymatic glucose sensor is 2657 μA mM^{-1} cm^{-2}. The detection limit was estimated to be 1.71 μM by $3s/\sigma$, where s and σ are the standard deviation of the background current and the slope of the calibration curve, respectively. The detection limit of the as-prepared CuO/Nafion/GCE is relatively low among the sensors, which is much lower than the normal blood glucose level of 4.4–6.6 mM,[45] indicating that the as-prepared CuO/Nafion/GCE electrode is suitable for the electrochemical detection of blood glucose. Note that the sensitivity of our present sensing system (nanoflowers) is higher than that of nanoleaves (see Fig. 6f) and other reported CuO materials,[46–52] as shown in Fig. S6 and Table S1 (ESI†). The relative standard deviation (RSD) of the amperometric response to 100 μM of glucose at +0.50 V is 2.88% for

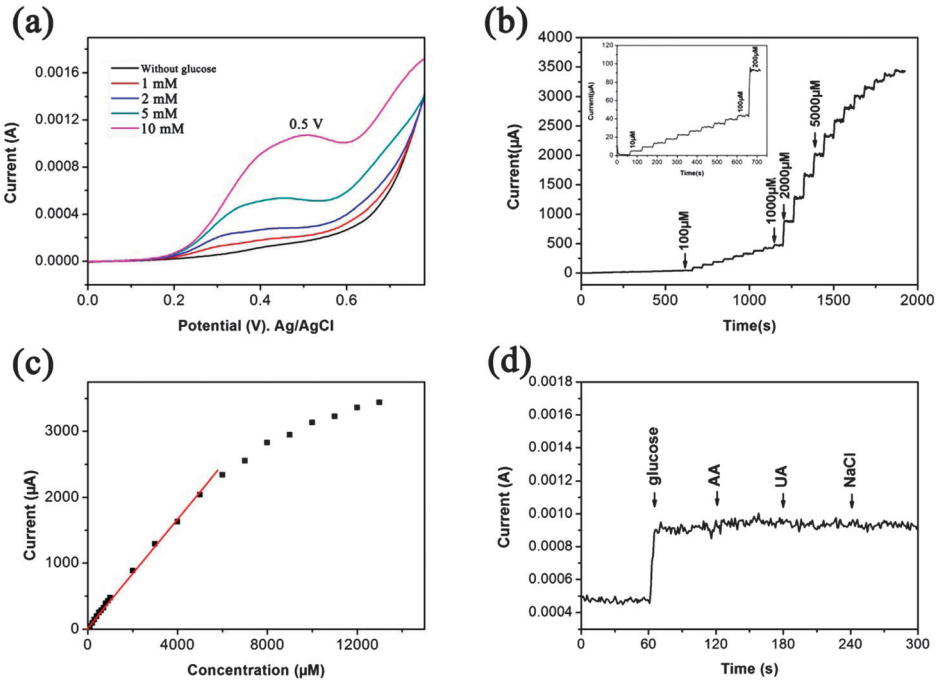

Fig. 7 (a) Linear sweep voltammograms collected for the as-prepared CuO/Nafion/GCE in a range of glucose concentrations between 0 and 10 mM; (b) amperometric response of CuO/Nafion/GCE with successive addition of different glucose to 0.1 M KOH at 0.50 V *vs.* Ag/AgCl; (c) current-glucose concentration calibration curve obtained for the as-prepared CuO/Nafion/GCE; (d) anti-interference property of CuO/NFs/GCE to the stepwise addition of 100 μM AA, 100 μM UA, and 100 μM NaCl, followed by the successive addition of 1000 μM glucose solutions.

5 successive measurements, indicating the good reproducibility of the as-prepared CuO/Nafion/GCE.

For a glucose sensor, interference is another important parameter which affects its electrochemical response because easily oxidative species such as ascorbic acid (AA), uric acid (UA) and sodium chloride (NaCl) usually co-exist with glucose in human blood. Herein, the electrochemical sensitivity of the above interfering species were also investigated using the as-prepared CuO/Nafion/GCE. Because the normal physiological level of glucose is substantially higher than that of the interfering agents,[53] the anti-interference effect of the modified as-prepared CuO/Nafion/GCE was tested by successive addition of 1000 μM glucose at +0.50 V *vs.* Ag/AgCl, followed by the additions of 100 μM AA, 100 μM UA and 100 μM NaCl in a 0.1 M KOH solution, as shown in Fig. 7d. It is clearly observed that an excellent glucose response was obtained, while insignificant current responses were seen for interfering species compared to glucose addition. The observations suggest that our as-synthesized hierarchical CuO nanostructures demonstrate an excellent specificity for glucose detection in the presence of normally co-existing interfering agents.

The exact mechanism for the oxidation of glucose on the CuO modified electrode in an alkaline medium is still uncertain. To date, the most accepted oxidation mechanism of glucose on the modified copper-based electrodes was suggested by Marioli and Kuwana.[54] Namely, the oxidation is generated by the deprotonation of the glucose and isomerization to its enediol form, followed by adsorption onto the electrode surface and oxidation by Cu(II) and Cu(III). Glucose oxidation occurred at a potential range of 0.40–0.80 V, where the oxidation wave for the Cu(II)/Cu(III) was demonstrated.[55–58] Herein, the Cu(III) species are proposed to act as an electron-transfer medium.[59,60] During cyclic voltammetric measurement, Cu(II) on an CuO electrode would be first oxidized to Cu(III) (eqn (1)). Then the oxidative Cu(III) could catalyze glucose oxidation to generate gluconolactone and then gluconolactone is further oxidized to glucose acid (eqn (2)). As schematically shown in Fig. 8, the electrochemical nonenzymatic detection of glucose reduction is assisted by the Cu(II)/Cu(III) redox couple. Thus, an enhanced catalytic current response on our CuO modified electrode in the

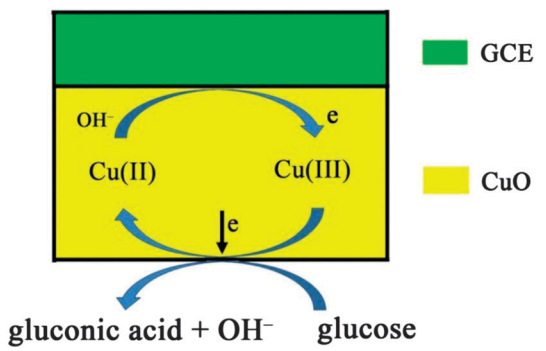

$$CuO + OH^- \rightarrow CuOOH + e \quad (1)$$

$$CuOOH + e + glucose \rightarrow CuO + OH^- + gluconic\ acid \quad (2)$$

Fig. 8 A schematic of the possible pathways during non-enzymatic electro-oxidation of glucose on CuO/NFs/GCE surface in alkaline medium.

presence of glucose solution and the response current depends on the glucose concentration (see Fig. 7b).

Here, the as-prepared bicomponent CuO hierarchical nanoflowers being multiple nanoparticle building blocks provide large interfaces (high surface area, see Fig. S7, ESI†), and could improve the diffusion of glucose molecules during kinetic electron transfer in the electrochemical process.[61] In addition, it has been well-demonstrated that the presence of highly active crystallographic planes can accelerate the chemical activity of crystals.[42,62] As reported previously in ref. 42, the (111) plane of CuO crystal is terminated with a Cu and O atomic layer, which gives rise to insufficient oxygen atoms coordination with positive Cu dangling bonds on the surface. So our bicomponent CuO hierarchical nanoflowers exposed with a number of highly active (111) planes would adsorb more OH^- ions and facilitate the transfer of electrons during the electrochemical process (eqn (1) and eqn (2)).

4. Conclusion

We have successfully demonstrated, for the first time, a facile, one-pot water/ethanol solution-phase transformation of $Cu_2(NO_3)(OH)_3$ precursors into well-defined 3D nanoparticle-aggregated bicomponent CuO hierarchical nanoflowers. We have revealed a sequential *in situ* dissolution–precipitation formation mechanism, in which water is a required reactant. Precise structural information for the precursory and intermediated crystals has been provided, and the transformation of the $Cu_2(NO_3)(OH)_3$ crystals into poly-crystalline CuO nanoflowers has been evidenced. We have also demonstrated that the controlled growth of monoclinic CuO nanostructures with different morphologies can be readily achieved by adjusting the volume ratio between water and ethanol. Such bicomponent CuO hierarchical nanoflower serve as a promising electrode material for a nonenzymatic glucose sensor showing a higher sensitivity of 2657 μA mM^{-1} cm^{-2}, a linear response in the concentration ranging from 10 μM to 5 mM at +0.50 V *vs.* Ag/AgCl and good selectivity against common interfering species. More importantly, the findings reveal that the different $Cu_xM_y(OH)_z$ (M = acidic radical) precursors synthesized in a water/ethanol reaction environment can be utilized to obtain new forms of CuO nanomaterials, and it is anticipated that precise control of the reaction environment would serve to optimize the structures and morphologies of CuO crystals. Experiments with different copper salts, such as $CuCl_2$, and $CuSO_4$, are in progress towards this goal.

Acknowledgements

This work was supported by the National Science Foundation of China (Grant 51272209), Natural Science Foundation of Shaanxi Province (Grant 2011JZ008), Youth Foundation of Shaanxi Province of China (Grant 2012JQ6007), Doctoral Fund of Ministry of Education of China (Grant20120201120051), and Fundamental Research Funds for the Central Universities of China.

Notes and references

1 Y. D. Yin, R. M. Rioux, C. K. Erdonmez, S. Hughes, G. A. Somorjai and A. P. Alivisatos, *Science*, 2004, **304**, 711.
2 P. Liu, Y. Wang, H. M. Zhang, T. C. An, H. G. Yang, Z. Y. Tang, W. P. Cai and H. J. Zhao, *Small*, 2012, **8**, 3664.
3 A. P. Alivisatos, *Science*, 1996, **271**, 933.
4 C. Burda, X. B. Chen, R. Narayanan and M. A. El-Sayed, *Chem. Rev.*, 2005, **105**, 1025.
5 Md. M. Rahman, A. J. S. Ahammad, J. H. Jin, S. J. Ahn and J. J. Lee, *Sensors*, 2010, **10**, 4855.
6 Y. S. Chaudhary, A. Agrawal, R. Shrivastav, V. R. Satsangi and D. Dass, *Int. J. Hydrogen Energy*, 2004, **29**, 131.
7 M. Yang, J. He, X. Hu, C. Yan and Z. Cheng, *Environ. Sci. Technol.*, 2011, **45**, 6088.
8 S. F. Zheng, J. S. Hu, L. S. Zhong, W. G. Song and L. J. Wan, *Chem. Mater.*, 2008, **20**, 3617.
9 L. B. Chen, N. Lu, C. M. Xu, H. C. Yu and T. H. Wang, *Electrochim. Acta*, 2009, **54**, 4198.
10 X. J. Zhang, W. H. Shi, J. X. Zhu, D. J. Kharistal, W. Y. Zhao, B. Si, H. H. Huang and Q. Y. Yan, *ACS Nano*, 2011, **5**, 2013.
11 G. L. Wang, J. C. Huang, S. L. Chen, Y. Y. Gao and D. X. Cao, *J. Power Sources*, 2011, **196**, 5756.
12 C. T. Hsieh, J. M. Chen, H. H. Lin and H. C. Shi, *Appl. Phys. Lett.*, 2003, **83**, 3383.
13 G. H. Qiu, S. Dharmarathna, Y. S. Zhang, N. Opembe, H. S. Huang and S. L. Suib, *J. Phys. Chem. C*, 2012, **116**, 468.
14 M. Y. Zhu and G. W. Diao, *Catal. Sci. Technol.*, 2012, **2**, 82.
15 M. Izaki, T. Shinagawa, K. T. Mizuno, Y. Ida, M. Inaba and A. Tasaka, *J. Phys. D: Appl. Phys.*, 2007, **40**, 3326.
16 L. Q. Lu and Y. Wang, *Electrochem. Commun.*, 2012, **14**, 82.
17 S. U. Son, I. K. Park, J. Park and T. Hyeon, *Chem. Commun.*, 2004, 778.
18 J. Liu, X. Huang, Y. Li, K. M. Sulieman, X. He and F. Sun, *Cryst. Growth Des.*, 2006, **6**, 16901.
19 X. Q. Wang, G. C. Xi, S. L. Xiong, Y. K. Liu, B. J. Xi, W. C. Yu and Y. T. Qian, *Cryst. Growth Des.*, 2007, **7**, 930.
20 H. M. Xiao, S. Y. Fu, L. P. Zhu, Y. Q. Li and G. Yang, *Eur. J. Inorg. Chem.*, 2007, 1966.
21 M. H. Cao, C. W. Hu, Y. H. Wang, Y. H. Guo, C. X. Guo and E. B. Wang, *Chem. Commun.*, 2003, 1884.
22 J. T. Zhang, J. F. Liu, Q. Peng, X. Wang and Y. Li, *Chem. Mater.*, 2006, **18**, 867.
23 C. H. B. Ng and W. Y. Fan, *J. Phys. Chem. C*, 2007, **111**, 9166.
24 A. Taubert, A. Uhlmann, A. Hedderich and K. Kirchhoff, *Inorg. Chem.*, 2008, **47**, 10758.
25 X. H. Liu, J. Zhang, Y. F. Kang, S. H. Wu and S. R. Wang, *CrystEngComm*, 2012, **14**, 620.
26 D. Q. Gao, G. J. Yang, J. Y. Li, J. Zhang, J. L. Zhang and D. S. Xue, *J. Phys. Chem. C*, 2010, **114**, 18347.
27 L. P. Xu, S. Sithambaram, Y. S. Zhang, C. H. Chen, L. Jin, R. Joesten and S. L. Suib, *Chem. Mater.*, 2009, **21**, 1253.
28 Q. Yu, H. W. Huang, R. Chen, P. Wang, H. S. Yang, M. X. Gao, X. S. Peng and Z. Z. Ye, *Nanoscale*, 2012, **4**, 2613.
29 S. H. Park and H. J. Kim, *J. Am. Chem. Soc.*, 2004, **126**, 14368.

30 J. M. Aguirre, A. Gutiérrez, O. Giraldo and J. Braz, *Chem. Soc.*, 2011, **22**, 546.
31 B. Liu and H. C. Zeng, *J. Am. Chem. Soc.*, 2004, **126**, 8124.
32 Z. M. Zhang, H. P. Sun, X. Q. Shao, D. F. Li, H. D. Yu and M. Y. Han, *Adv. Mater.*, 2005, **17**, 42.
33 A. Taubert, A. Uhlmann, A. Hedderich and K. Kirchhoff, *Inorg. Chem.*, 2008, **47**, 10758.
34 B. Liu, *Nanoscale*, 2012, **4**, 7194.
35 S. H. Lee, Y. S. Her and E. Matijević, *J. Colloid Interface Sci.*, 1997, **186**, 193.
36 J. F. Xu, W. Ji, Z. X. Shen, W. S. Li, S. H. Tang, X. R. Ye, D. Z. Jia and X. Q. Xin, *J. Raman Spectrosc.*, 1999, **30**, 413.
37 D. P. Volanti, M. O. Orlandi, J. Andrés and E. Longo, *CrystEngComm*, 2010, **12**, 1696.
38 Y. Cudennec and A. Lecerf, *Solid State Sci.*, 2003, **5**, 1471.
39 D. P. Sing, A. K. Ojha and O. N. Stivastava, *J. Phys. Chem. C*, 2009, **113**, 3409.
40 Y. Cudennee, A. Lecerf and Y. Gérault, *C. R. Acad. Sci., Ser. IIc: Chim*, 2000, **3**, 661.
41 J. C. Park, J. H. Kim, H. Kwon and H. Song, *Adv. Mater.*, 2009, **21**, 803.
42 Z. Y. Fei, P. Lu, X. Z. Feng, B. Sun and W. J. Ji, *Catal. Sci. Technol.*, 2012, **2**, 1705.
43 J. Wang, M. Musameh and Y. H. Lin, *J. Am. Chem. Soc.*, 2003, **125**, 2408.
44 L. C. Jiang and W. D. Zhang, *Biosens. Bioelectron.*, 2010, **25**, 1402.
45 K. M. E. Khatiba and R. M. A. Hameed, *Biosens. Bioelectron.*, 2011, **26**, 3542.
46 J. Yang, L. C. Jiang, W. D. Zhang and S. Gunasekarana, *Talanta*, 2010, **82**, 25.
47 S. Liu, J. Q. Tian, L. Wang, X. Y. Qin, Y. W. Zhang, Y. L. Luo, A. M. Asiri, A. O. Al-Youbi and X. P. Sun, *Catal. Sci. Technol.*, 2012, **2**, 813.
48 Z. Y. Yang, J. S. Feng, J. S. Qiao, Y. M. Yan, Q. Y. Yu and K. N. Sun, *Anal. Methods*, 2012, **4**, 1924.
49 X. Wang, C. Hu, H. Liu, G. Du, X. He and Y. Xi, *Sens. Actuators, B*, 2010, **144**, 220.
50 E. Reitz, W. Z. Jia, M. Gentile, Y. Wang and Y. Lei, *Electroanalysis*, 2008, **20**, 2482.
51 W. Wang, L. L. Zhang, S. F. Tong, X. Li and W. B. Song, *Biosens. Bioelectron.*, 2009, **25**, 708.
52 T. Soejima, H. Yagyu, N. Kimizuka and S. Ito, *RSC Adv.*, 2011, **1**, 187.
53 L. M. Li, Z. F. Du, S. A. Liu, Q. Y. Hao, Y. G. Wang, Q. H. Li and T. H. Wang, *Talanta*, 2010, **82**, 1637.
54 J. M. Marioli and T. Kuwana, *Electrochim. Acta*, 1992, **37**, 1187.
55 Z. J. Zhuang, X. D. Su, H. Y. Yuan, Q. Sun, D. Xiao and M. M. F. Choi, *Analyst*, 2008, **133**, 126.
56 M. Z. Luo and R. P. Baldwin, *J. Electroanal. Chem.*, 1995, **387**, 87.
57 N. Torto, T. Ruzgas and L. Gorton, *J. Electroanal. Chem.*, 1999, **464**, 252.
58 A. J. Wang, J. J. Feng, Z. H. Li, Q. C. Liao, Z. Z. Wang and J. R. Chen, *CrystEngComm*, 2012, **14**, 1289.
59 T. R. L. C. Paixao, D. Corbo and M. Bertotti, *Anal. Chim. Acta*, 2002, **472**, 123.
60 X. H. Kang, Z. B. Mai, X. Y. Zou, P. X. Cai and J. Y. Mo, *Anal. Biochem.*, 2007, **363**, 143.
61 S. K. Meher and G. R. Rao, *Nanoscale*, 2013, **5**, 2089.
62 N. Tian, Z. Y. Zhou, S. G. Sun, Y. Ding and Z. L. Wang, *Science*, 2007, **316**, 732.